

# **Electronic states in oxidized Na<sub>x</sub>CoO<sub>2</sub> as revealed by X-ray absorption spectroscopy coupled with *ab initio* calculation**

Hideharu Niwa<sup>a-c,\*</sup>, Kazuyuki Higashiyama<sup>a,b</sup>, Kaoru Amaha<sup>a</sup>, Wataru Kobayashi<sup>a-c</sup>,  
Yutaka Moritomo<sup>a-c,\*</sup>

<sup>a</sup>Graduate School of Pure and Applied Science, University of Tsukuba, Tsukuba 305-8571,  
Japan

<sup>b</sup>Faculty of Pure and Applied Science, University of Tsukuba, Tsukuba 305-8571, Japan

<sup>c</sup>Tsukuba Research Center for Energy Materials Science (TREMS), University of  
Tsukuba, Tsukuba 305-8571, Japan

Contact information:

Hideharu Niwa / Yutaka Moritomo

Faculty of Pure and Applied Science,

Univ. of Tsukuba, Tennodai 1-1-1, Tsukuba 305-8571, Japan

Tel.; +81-29-853-4216 / +81-29-853-4337

E-mail: niwa.hideharu.ga@u.tsukuba.ac.jp / moritomo.yutaka.gf@u.tsukuba.ac.jp

## Abstract

Layered cobalt oxides are promising cathode materials for sodium ion secondary batteries (SIBs). By combined study of the X-ray absorption spectroscopy (XAS) around the O *K*-edge and *ab initio* calculation, we investigated the electronic state of the  $\text{Na}_x\text{CoO}_2$  with different oxidization state, *i.e.*, in O3- $\text{Na}_{0.91}\text{CoO}_2$  ( $\text{CoO}_2^{-0.91}$ ) and P2- $\text{Na}_{0.66}\text{CoO}_2$  ( $\text{CoO}_2^{-0.66}$ ). The O *K*-edge spectra in the pre-edge (529 – 536 eV) region shows significant change with oxidization of  $\text{Na}_x\text{CoO}_2$ . In O3- $\text{Na}_{0.91}\text{CoO}_2$ , the spectra shows an intense band (B band) at 531 eV. In P2- $\text{Na}_{0.66}\text{CoO}_2$ , the spectral weight of the B band increases and a new band (A band) appears at 530 eV. These spectral changes are qualitatively reproduced by the calculated partial density of states (pDOSs) of O3- $\text{NaCoO}_2$  and P2- $\text{Na}_{1/2}\text{CoO}_2$ . These results indicate that the electrons are partially removed from the O *2p* state with oxidization of  $\text{Na}_x\text{CoO}_2$ .

## 1. Introduction

Sodium ion secondary batteries (SIBs) have attracted much attention as promising candidates for next-generation batteries beyond lithium ion secondary batteries [1-6]. Due to the abundancy and low cost of sodium, SIBs are applicable to large-scale electrical energy storage systems and electric vehicles. Among several types of cathode materials for SIBs, layered cobalt oxides with O3- and P2-type structures show promising electrochemical properties [7, 8]. Both the O3- and P2-type structures consist of the  $\text{CoO}_2$  sheet of edge-sharing  $\text{CoO}_6$  octahedra. In the charge process,  $\text{Na}^+$  is extracted between the neighboring  $\text{CoO}_2$  sheets and electrons are removed from the  $\text{CoO}_2$  sheet. Up to now, it is considered that electrons are removed from Co in the  $\text{CoO}_2$  sheet. However, several groups proposed that the electrons are partly removed from the O *2p* state [9-11].

XAS is a powerful tool to investigate the electronic states of the battery materials. Especially, soft XAS provides element-specific information sensitive to valence states of  $3d$  transition metals ( $M_s$ ) and ligand oxygens, because the energy range covers dipole-allowed transitions at the  $M$   $L$ -edge and  $O$   $K$ -edge. For  $O$   $K$ -edge XAS, the *ab initio* calculation is considered to be a good approach because the spectra is nearly free from the multiplet and charge-transfer effects [12]. Recently, *in situ/operando* soft X-ray spectroscopy is becoming a powerful tool to investigate the variation of the electronic state of the battery materials during electrochemical reactions [13, 14]. There, however, exist few reports [15, 16] on the battery materials, since the *in situ/operando* soft X-ray spectroscopy needs a vacuum compatible batteries cell. On the other hand, the number of *ex situ*  $O$   $K$ -edge XAS researches on binary or ternary transition metal layered oxides have been increasing [9-11, 17, 18].

In this paper, variation of the electronic state of the  $\text{Na}_x\text{CoO}_2$  ( $\text{CoO}_2$  sheet) with oxidization was investigated by combined study of the  $O$   $K$ -edge XAS and *ab initio* calculation. The  $O$   $K$ -edge spectra in the pre-edge (529 – 536 eV) region show significant change between O3- $\text{Na}_{0.91}\text{CoO}_2$  ( $\text{CoO}_2^{-0.91}$ ) and P2- $\text{Na}_{0.66}\text{CoO}_2$  ( $\text{CoO}_2^{-0.66}$ ). The spectral changes are qualitatively reproduced by the pDOSs of O3- $\text{NaCoO}_2$  and P2- $\text{Na}_{1/2}\text{CoO}_2$ . These results indicate that the electrons are partially removed from the  $O$   $2p$  state with oxidization of the  $\text{Na}_x\text{CoO}_2$ .

## 2. Experimental and calculation details

### 2.1 Sample preparation

O3- and P2-type  $\text{Na}_x\text{CoO}_2$  were prepared by solid state reaction. In the O3-type compound,  $\text{Na}_2\text{O}_2$  and  $\text{Co}_3\text{O}_4$  were mixed in a 1.25: 1 atomic ratio and calcined at 823 K

for 16 h in O<sub>2</sub>. Then, the product was finely ground, and again calcined in the same condition. In the P2-type compound, Na<sub>2</sub>CO<sub>3</sub> and Co<sub>3</sub>O<sub>4</sub> were mixed in a 0.7:1 atomic ratio and calcined at 1073 K for 12 h in air. The Na concentrations (*x*) were determined by the Rietveld analyses of the synchrotron-radiation X-ray powder diffraction pattern.

## 2.2 X-ray diffraction and Rietveld analysis

Synchrotron-radiation X-ray powder diffraction (XRD) measurements were performed at the BL-8A beamline of the Photon Factory, KEK. The samples were finely ground and placed in  $\phi$ 0.3 mm glass capillaries. The capillaries were sealed and mounted on the Debye-Scherrer camera. The powder diffraction patterns were detected with an imaging plate. The exposure time was 5 minutes. The wavelength (= 0.68903 Å) of the X-ray was calibrated by the lattice constant of standard CeO<sub>2</sub> powders. The XRD patterns of the O3-type compound was analyzed by the Rietveld method with a trigonal model ( $R\bar{3}m$ ;  $Z= 3$ , hexagonal setting). The XRD patterns of the P2-type compound was analyzed by the Rietveld method with a hexagonal model ( $P63/mmc$ ;  $Z= 2$ ). X-ray diffraction patterns and Rietveld refinement profiles are shown in Figure S1 and S2 in the Supplementary Materials. In both compounds, no traces of impurities nor secondary phases were observed. The obtained structural parameters are listed in Table 1 and 2.

**Table 1.** Structural parameters of O3-Na<sub>0.91</sub>CoO<sub>2</sub> at 300 K refined by the Rietveld method ( $R\bar{3}m$ ,  $Z=3$ ). *g* and *B* are occupancy and atomic displacement parameter, respectively. Lattice constants are  $a = 2.88795(5)$  Å,  $c = 15.59923(32)$  Å. Reliable parameters are  $R_{wp} = 5.15\%$ ,  $R_1 = 5.26\%$ , and  $S = 5.54$ .

atom	site	<i>g</i>	<i>x</i>	<i>y</i>	<i>z</i>	<i>B</i>
------	------	----------	----------	----------	----------	----------

Na	3a	0.905(4)	0	0	0	0.09(4)
Co	3b	1	0	0	0.5	0.17(1)
O	6c	1	0	0	0.2281(1)	0.37(4)

**Table 2.** Structural parameters of P2-Na<sub>0.66</sub>CoO<sub>2</sub> at 300K refined by the Rietveld method (*P*63/mmc; *Z* = 2). *g* and *B* are occupancy and atomic displacement parameter, respectively. Lattice constants are *a* = 2.82842(11) Å, *c* = 10.94605(65) Å. Reliable parameters are *R*<sub>wp</sub> = 5.90%, *R*<sub>I</sub> = 7.46%, and *S* = 6.12.

atom	site	<i>g</i>	<i>x</i>	<i>y</i>	<i>z</i>	<i>B</i>
Na1	2b	0.246(7)	0	0	0.25	3.88(37)
Na2	2d	0.418(9)	1/3	2/3	0.75	3.88
Co	2a	1	0	0	0	0.30(3)
O	4f	1	1/3	2/3	0.0840(4)	0.66(9)

### 2.3 X-ray absorption spectroscopy

O K-edge and Co L-edge XAS recorded in the total electron yield (TEY) mode were measured at soft X-ray beam line BL12 of the SAGA Light Source, Japan. The spectra were obtained at room temperature in a vacuum of  $2 \times 10^{-8}$  Torr. The TEY-XAS spectra were obtained by dividing the sample drain current by the gold mesh current of the incident X-ray intensity. The energy resolution ( $E/\Delta E$ ) was over 2000. The O K-edge XAS recorded in the partial fluorescence yield (PFY) mode were conducted at TLS BL08B1 beamline at the NSRRC in Taiwan. The PFY-XAS spectra were obtained using a silicon drift detector (SDD, Amptek) at room temperature. The energy resolution was over 2000.

### 2.4 First principles calculation

The pDOSs were calculated for O3-NaCoO<sub>2</sub>, P2-NaCoO<sub>2</sub>, and P2-Na<sub>1/2</sub>CoO<sub>2</sub> using

density functional theory with the plane-wave self-consistent field (PWscf) package [19]. A plane wave basis set with a cutoff energy of 612 eV was chosen, and the projector-augmented-wave potentials were used. We adopted the exchange-correlation functional of Perdew-Burke-Ernzerhof type within generalized gradient approximation. Local spin density approximation was used to take account of electron spin. In the calculation of O3-NaCoO<sub>2</sub>, we used the lattice constant ( $a$  and  $c$ ) and atomic coordinate ( $z$ ) of O3-Na<sub>0.91</sub>CoO<sub>2</sub> (Table 1) without structural optimization. In the calculation of P2-NaCoO<sub>2</sub>, we used the lattice constant ( $a$  and  $c$ ) and atomic coordinate ( $z$ ) of P2-Na<sub>0.66</sub>CoO<sub>2</sub> (Table 2) without structural optimization. The Na ions were placed in the Na(2) sites because the total energy is lower by 117 meV/FU than that for the Na(1) site. In the calculation of P2-Na<sub>1/2</sub>CoO<sub>2</sub>,  $1 \times 2 \times 1$  supercell was built based on the hexagonal unit cell. The Na ions were alternately placed in the Na(2) sites, as shown in the inset of Fig. 3(b). We used the lattice constant ( $a$  and  $c$ ) and atomic coordinate ( $z$ ) of P2-Na<sub>0.66</sub>CoO<sub>2</sub> (Table 2) without structural optimization. Brillouin-zone sampling for the scf (DOS) calculations was made using the Monkhorst-Pack method with  $12 \times 12 \times 12$  ( $36 \times 36 \times 36$ ) k points for P2-NaCoO<sub>2</sub>,  $12 \times 12 \times 8$  ( $36 \times 36 \times 24$ ) for O3-NaCoO<sub>2</sub> and  $12 \times 6 \times 12$  ( $36 \times 18 \times 36$ ) for P2-Na<sub>1/2</sub>CoO<sub>2</sub>. The calculation shows good convergence with respect to the cutoff energy and k point.

### 3. Results and Discussion

#### 3.1 Co L-edge XAS spectra

Figure 1(a) shows Co L-edge spectra of O3-Na<sub>0.91</sub>CoO<sub>2</sub> and P2-Na<sub>0.66</sub>CoO<sub>2</sub>. Two intense absorptions,  $L_2$  and  $L_3$ , are observed.  $L_2$  ( $L_3$ ) is ascribed to the dipole-allowed transition from the Co  $2p_{1/2}$  (Co  $2p_{3/2}$ ) to Co  $3d$  orbitals. Spectral feature of P2-Na<sub>0.66</sub>CoO<sub>2</sub> is almost

the same as that of O3-Na<sub>0.91</sub>CoO<sub>2</sub>, except for slight blue-shift of the peak energies. The energy shift is consistent with Co L-edge XAS of Li<sub>x</sub>CoO<sub>2</sub> reported by Mizokawa *et al* [20]. As the concentration of Li decreases, the 2p<sub>3/2</sub> (L<sub>3</sub>) peak energy shifts to higher photon energy (blue shift). Therefore, the blue-shift suggests increases in the Co valence of the Na<sub>x</sub>CoO<sub>2</sub>.

### 3.2 O K-edge XAS spectra

Figure 1(b) shows O K-edge spectra of O3-Na<sub>0.91</sub>CoO<sub>2</sub> and P2-Na<sub>0.66</sub>CoO<sub>2</sub>. The spectra were normalized at 550 eV. For the convenience of explanation, we divide the spectra into the pre-edge (529 - 536 eV) and main (> 536 eV) regions. In the pre-edge region (529 – 534 eV), an intense peak (labeled as peak B) is observed around 531 eV in both the compounds. In P2-Na<sub>0.66</sub>CoO<sub>2</sub>, an additional peak (labeled as peak A) and its shoulder peak A' appears around 530 eV and 529 eV, respectively. The pre-edge peak profiles are similar to that of Li<sub>x</sub>CoO<sub>2</sub> [20]. The peaks A', A and B are ascribed to the transitions from the O 1s to O 2p orbital. The O 2p state is strongly hybridized with the Co 3d state. Several studies on Na<sub>0.5</sub>CoO<sub>2</sub> [21] and Na<sub>x</sub>Co<sub>2/3</sub>Mn<sub>1/3</sub>O<sub>2</sub> [10] have reported that O K-edge XAS spectra show the peak C around 535 eV and are attributed to transition to hybridized states between O 2p and Na 3p. Bulk-sensitive O K-edge spectra in partial fluorescence yield mode (Figure S3, Supplementary Materials) showed that the intensity of peak C is weaker than that in total electron yield mode. Therefore, the peak C is also possible to be attributed to surface species. The broad absorption in the main region (> 556 eV) is ascribed to the transition from the O 1s to the O 2p – Co 4sp hybridized state [12]. In the present study, we focused on peaks A', A and B to discuss the electronic states with oxidation of the CoO<sub>2</sub> sheet.

Figure 2 shows magnified O K-edge spectra recorded in TEY mode of (a) O3- $\text{Na}_{0.91}\text{CoO}_2$  and (b) P2- $\text{Na}_{0.66}\text{CoO}_2$  around the peaks A', A and B. To evaluate the spectral weights of the peaks A and B, least-squares fitting with three Gauss functions and step function-type background was performed. The spectral weight of the peak B increases from 0.36 in O3- $\text{Na}_{0.91}\text{CoO}_2$  to 0.85 in P2- $\text{Na}_{0.66}\text{CoO}_2$ . Normalization method and background type in the least-squares fitting of O K-edge TEY-XAS spectra do not affect the resultant trend that the spectral weight of peak B increased from O3- $\text{Na}_{0.91}\text{CoO}_2$  to P2- $\text{Na}_{0.66}\text{CoO}_2$  (Figures S3, S4 and Table S1, Supplementary Materials). The analyses of O K-edge PFY-XAS spectra also showed the same tendency (Figures S3, S5 and Table S2, Supplementary Materials). Therefore, the spectral variation suggests that the unoccupied O  $2p$  state increases with oxidization of the  $\text{Na}_x\text{CoO}_2$ .

### 3.3 Calculation of pDOS

We will discuss above-observed spectral change between O3- $\text{Na}_{0.91}\text{CoO}_2$  and P2- $\text{Na}_{0.66}\text{CoO}_2$  in terms of the first principles calculation. Figure 3(a) shows Co (broken blue curves), O (solid curves), and Na (broken red curves) pDOSs in O3- $\text{NaCoO}_2$ . Both the O3- and P2-type structures consist of the  $\text{CoO}_2$  sheet of edge-sharing  $\text{CoO}_6$  octahedra, causing crystal field splitting of the Co  $3d$  orbital into the lower-lying  $t_{2g}$  and upper-lying  $e_g$  ones. The  $t_{2g}$  and  $e_g$  states correspond to the bands around -0.8 and 1.6 eV. The  $t_{2g}$  band is fully occupied while the  $e_g$  band is unoccupied. The system is non-magnetic insulator with a gap of  $\sim 1$  eV. We observed a strong O  $2p$  – Co $3d$  hybridization in both the  $t_{2g}$  and  $e_g$  bands. The electronic structure around the fermi energy ( $E_f$ ) is governed by that of the  $\text{CoO}_2$  sheets, since the Na pDOS is negligible in this energy region. The peak B observed in the O K-edge XAS [Fig.2(a)] is assigned to the transition from the O  $1s$  to the  $e_g$  band

around 1.6 eV. Here, we note that the oscillator strength of the transition is proportional to the unoccupied pDOS intensity (=1.36 state/FU) of the oxygen component. We further confirmed that calculated pDOS of P2-NaCoO<sub>2</sub> (Figure S6, Supplementary Materials) is almost the same as that of O3-NaCoO<sub>2</sub>: the amount of oxygen pDOS intensity in the unoccupied  $e_g$  band differs by only  $\sim 1\%$  for both structures. This indicates that the pDOS is insensitive to the stacking sequence of the CoO<sub>2</sub> sheet as well as the structural parameters when compared with the same Na content.

Figure 3(b) shows pDOS of P2-Na<sub>1/2</sub>CoO<sub>2</sub>. The  $t_{2g}$  and  $e_g$  bands correspond to the bands around -0.6 and 2.0 eV. The oxidization (hole-doping) of the CoO<sub>2</sub> sheet causes spin polarization. Especially, the down-spin  $t_{2g}$  band crosses  $E_f$ , and hence, is partially unoccupied. This is consistent with the Co  $L$ -edge spectra [Fig.1(a)], which suggests increases in the Co valence. The system is ferromagnetic metal with Co spin moment of 0.51  $\mu_B$ . The electronic structure is consistent with the literature [22]. We observed strong O  $2p$  – Co  $3d$  hybridization in both the  $t_{2g}$  and  $e_g$  bands. The peak A [Fig.2(b)] is assigned to the transition from the O  $1s$  to the unoccupied down-spin  $t_{2g}$  band ( $> E_f$ ). On the other hand, the peak B is assigned to the transition from the O  $1s$  to the  $e_g$  band around 2.0 eV. Its oscillator strength is proportional to the unoccupied pDOS intensity (=1.62 state/FU) of the oxygen component.

The first principles band calculation qualitatively reproduces the variation of the O K-edge spectra between O3-Na<sub>0.91</sub>CoO<sub>2</sub> and P2-Na<sub>0.66</sub>CoO<sub>2</sub>. First, the spectral weight of the peak B increases with oxidization of the Na<sub>x</sub>CoO<sub>2</sub> (CoO<sub>2</sub> sheet) from 0.36 in O3-Na<sub>0.91</sub>CoO<sub>2</sub> (CoO<sub>2</sub><sup>-0.91</sup>) to 0.55 in P2-Na<sub>0.66</sub>CoO<sub>2</sub> (CoO<sub>2</sub><sup>-0.66</sup>). This is consistent with the increase in the oxygen component of the  $e_g$  band from 1.36 state/FU in O3-NaCoO<sub>2</sub> to 1.62 state/FU in P2-Na<sub>1/2</sub>CoO<sub>2</sub>. Secondly, in P2-Na<sub>0.66</sub>CoO<sub>2</sub>, an additional peak A appears

at 530 eV. The peak A corresponds to the transition to the unoccupied state of the down-spin  $t_{2g}$  band. Thus, the combined study of the O K-edge XAS and *ab initio* band calculation reveals that the electrons are partially removed from the O  $2p$  state with the oxidization (hole-doping) of the  $\text{Na}_x\text{CoO}_2$  ( $\text{CoO}_2$  sheet).

#### 4. Conclusions

We performed a combined study of the O K-edge XAS and *ab initio* calculation on the electronic state of  $\text{Na}_x\text{CoO}_2$ . The *ab initio* calculation qualitatively reproduces the variation of the O K-edge spectra between O3- $\text{Na}_{0.91}\text{CoO}_2$  and P2- $\text{Na}_{0.66}\text{CoO}_2$ . Our analysis reveals that the electrons are partially removed from the O  $2p$  state with oxidization of the  $\text{Na}_x\text{CoO}_2$  ( $\text{CoO}_2$  sheet). We emphasize that our approach by combined study between experiments and calculations on the interpretation of the O K-edge spectra is easily applicable to the other materials.

#### Acknowledgements

This work was supported by JSPS KAKENHI (Grant Number JP17H0113 and JP16K20940 ). The X-ray powder diffraction experiments were performed under the approval of the Photon Factory Program Advisory Committee (Proposal No. 2014G507). The TEY-XAS experiments using synchrotron radiation were performed at the beamline BL12 of the SAGA Light Source with the approval of the Kyushu Synchrotron Light Research Center (Proposal No. 1604015R). The authors thank D. Yoshimura and E. Kobayashi for their technical supports during XAS measurements at SAGA Light Source and J. Okamoto, Y.-Y. Chu, A. Singh, and D.-J. Huang at NSRRC. Part of the *ab initio* calculation was performed using the supercomputing resources at Cyberscience Center,

Tohoku University.

## References

- [1] N. Yabuuchi, K. Kubota, M. Dahbi, S. Komaba, Research development on sodium-ion batteries, *Chem. Rev.* 114 (2014) 11636–11682. doi:10.1021/cr500192f.
- [2] M.D. Slater, D. Kim, E. Lee, C.S. Johnson, Sodium-ion batteries, *Adv. Funct. Mater.* 23 (2013) 947–958. doi:10.1002/adfm.201200691.
- [3] S.W. Kim, D.H. Seo, X. Ma, G. Ceder, K. Kang, Electrode materials for rechargeable sodium-ion batteries: Potential alternatives to current lithium-ion batteries, *Adv. Energy Mater.* 2 (2012) 710–721. doi:10.1002/aenm.201200026.
- [4] J.W. Choi, D. Aurbach, Promise and reality of post-lithium-ion batteries with high energy densities, *Nat. Rev. Mater.* 1 (2016) 16013. doi:10.1038/natrevmats.2016.13.
- [5] D. Kundu, E. Talaie, V. Duffort, L.F. Nazar, The emerging chemistry of sodium ion batteries for electrochemical energy storage, *Angew. Chemie - Int. Ed.* 54 (2015) 3432–3448. doi:10.1002/anie.201410376.
- [6] J.-Y. Hwang, S.-T. Myung, Y.-K. Sun, Sodium-ion batteries: present and future, *Chem. Soc. Rev.* 46 (2017) 3529–3614. doi:10.1039/C6CS00776G.
- [7] Y. Lei, X. Li, L. Liu, G. Ceder, Synthesis and Stoichiometry of Different Layered Sodium Cobalt Oxides, *Chem. Mater.* 26 (2014) 5288–5296. doi:10.1021/cm5021788.
- [8] M.H. Han, E. Gonzalo, G. Singh, T. Rojo, A comprehensive review of sodium layered oxides: powerful cathodes for Na-ion batteries, *Energy Environ. Sci.* 8 (2015) 81–102. doi:10.1039/C4EE03192J.
- [9] Y. Nanba, T. Iwao, B.M. de Boisse, W. Zhao, E. Hosono, D. Asakura, H. Niwa, H. Kiuchi, J. Miyawaki, Y. Harada, M. Okubo, A. Yamada, Redox Potential Paradox in

$\text{Na}_x\text{MO}_2$  for Sodium-Ion Battery Cathodes, *Chem. Mater.* 28 (2016) 1058–1065. doi:10.1021/acs.chemmater.5b04289.

[10] J.-H. Cheng, C.-J. Pan, J.-F. Lee, J.-M. Chen, M. Guignard, C. Delmas, D. Carlier, B.-J. Hwang, Simultaneous Reduction of  $\text{Co}^{3+}$  and  $\text{Mn}^{4+}$  in  $\text{P2-Na}_{2/3}\text{Co}_{2/3}\text{Mn}_{1/3}\text{O}_2$  As Evidenced by X-ray Absorption Spectroscopy during Electrochemical Sodium Intercalation, *Chem. Mater.* 26 (2014) 1219–1225. doi:10.1021/cm403597h.

[11] M. Okubo, A. Yamada, Molecular Orbital Principles of Oxygen-Redox Battery Electrodes, *ACS Appl. Mater. Interfaces.* 9 (2017) 36463–36472. doi:10.1021/acsami.7b09835.

[12] Frank de Groot, Akio Kotani, Core level spectroscopy of solids, (CRC Press, Boca Raton, FL, 2008).

[13] X. Liu, W. Yang, Z. Liu, Recent Progress on Synchrotron-Based In Situ Soft X-ray Spectroscopy for Energy Materials., *Adv. Mater.* 26 (2014) 7710–7729. doi:10.1002/adma.201304676.

[14] R. Toyoshima, H. Kondoh, *In-situ* observations of catalytic surface reactions with soft x-rays under working conditions, *J. Phys. Condens. Matter.* 27 (2015) 83003. doi:10.1088/0953-8984/27/8/083003.

[15] D. Asakura, E. Hosono, H. Niwa, H. Kiuchi, J. Miyawaki, Y. Nanba, M. Okubo, H. Matsuda, H. Zhou, M. Oshima, Y. Harada, *Operando* soft x-ray emission spectroscopy of  $\text{LiMn}_2\text{O}_4$  thin film involving Li-ion extraction/insertion reaction, *Electrochem. Commun.* 50 (2015) 93–96. doi:10.1016/j.elecom.2014.09.015.

[16] H. Niwa, H. Kiuchi, J. Miyawaki, Y. Harada, M. Oshima, Y. Nabae, T. Aoki, *Operando* soft X-ray emission spectroscopy of iron phthalocyanine-based oxygen reduction catalysts, *Electrochem. Commun.* 35 (2013) 57–60.

doi:10.1016/j.elecom.2013.08.003.

[17] C. Ma, J. Alvarado, J. Xu, R.J. Clément, M. Kodur, W. Tong, et al., Exploring Oxygen Activity in the High Energy P2-Type  $\text{Na}_{0.78}\text{Ni}_{0.23}\text{Mn}_{0.69}\text{O}_2$  Cathode Material for Na-Ion Batteries, *J. Am. Chem. Soc.* 139 (2017) 4835–4845. doi:10.1021/jacs.7b00164.

[18] S. Hy, W.-N. Su, J.-M. Chen, B.-J. Hwang, Soft X-ray Absorption Spectroscopic and Raman Studies on  $\text{Li}_{1.2}\text{Ni}_{0.2}\text{Mn}_{0.6}\text{O}_2$  for Lithium-Ion Batteries, *J. Phys. Chem. C* 116 (2012) 25242–25247. doi:10.1021/jp309313m.

[19] P. Giannozzi, S. Baroni, N. Bonini, M. Calandra, R. Car, C. Cavazzoni, et al., QUANTUM ESPRESSO: A modular and open-source software project for quantum simulations of materials, *J. Phys. Condens. Matter* 21 (2009). doi:10.1088/0953-8984/21/39/395502.

[20] T. Mizokawa, Y. Wakisaka, T. Sudayama, C. Iwai, K. Miyoshi, J. Takeuchi, et al., Role of oxygen holes in  $\text{Li}_x\text{CoO}_2$  revealed by soft X-ray spectroscopy, *Phys. Rev. Lett.* 111 (2013) 1–5. doi:10.1103/PhysRevLett.111.056404.

[21] W.B. Wu, D.J. Huang, J. Okamoto, A. Tanaka, H.J. Lin, F.C. Chou, A. Fujimori, C.T. Chen, Orbital symmetry and electron correlation in  $\text{Na}_x\text{CoO}_2$ , *Phys. Rev. Lett.* 94 (2005) 3–6. doi:10.1103/PhysRevLett.94.146402.

[22] D.J. Singh, Electronic structure of  $\text{NaCo}_2\text{O}_4$ , *Phys. Rev. B* 61 (2000) 13397–13402. doi:10.1103/PhysRevB.61.13397.

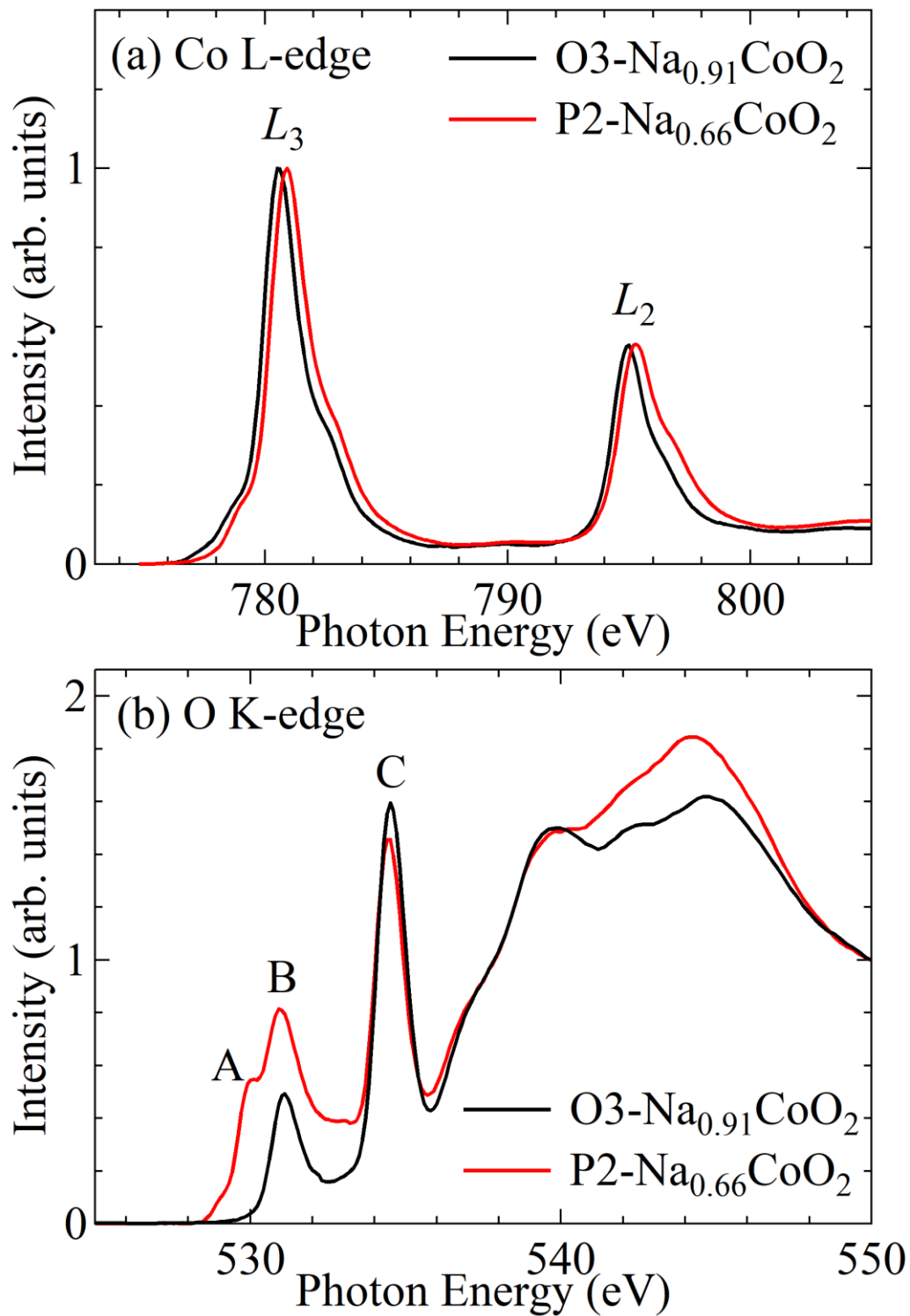


**Figure 1.** (a) Co L-edge and (b) O K-edge spectra recorded in TEY mode of O3- $\text{Na}_{0.91}\text{CoO}_2$  and P2- $\text{Na}_{0.66}\text{CoO}_2$ . The O K-edge spectra were normalized to have the same total area (526 – 550 eV).

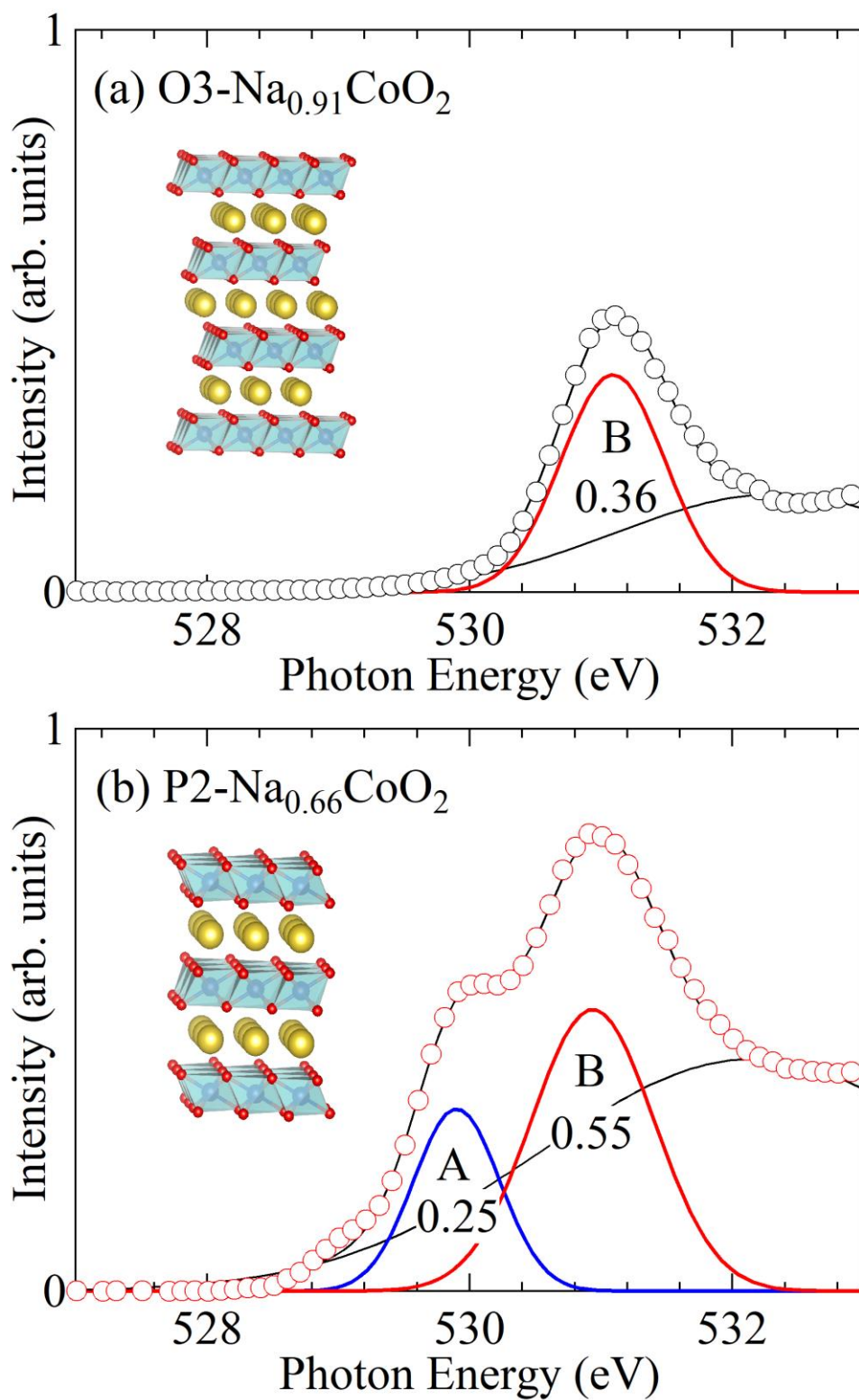
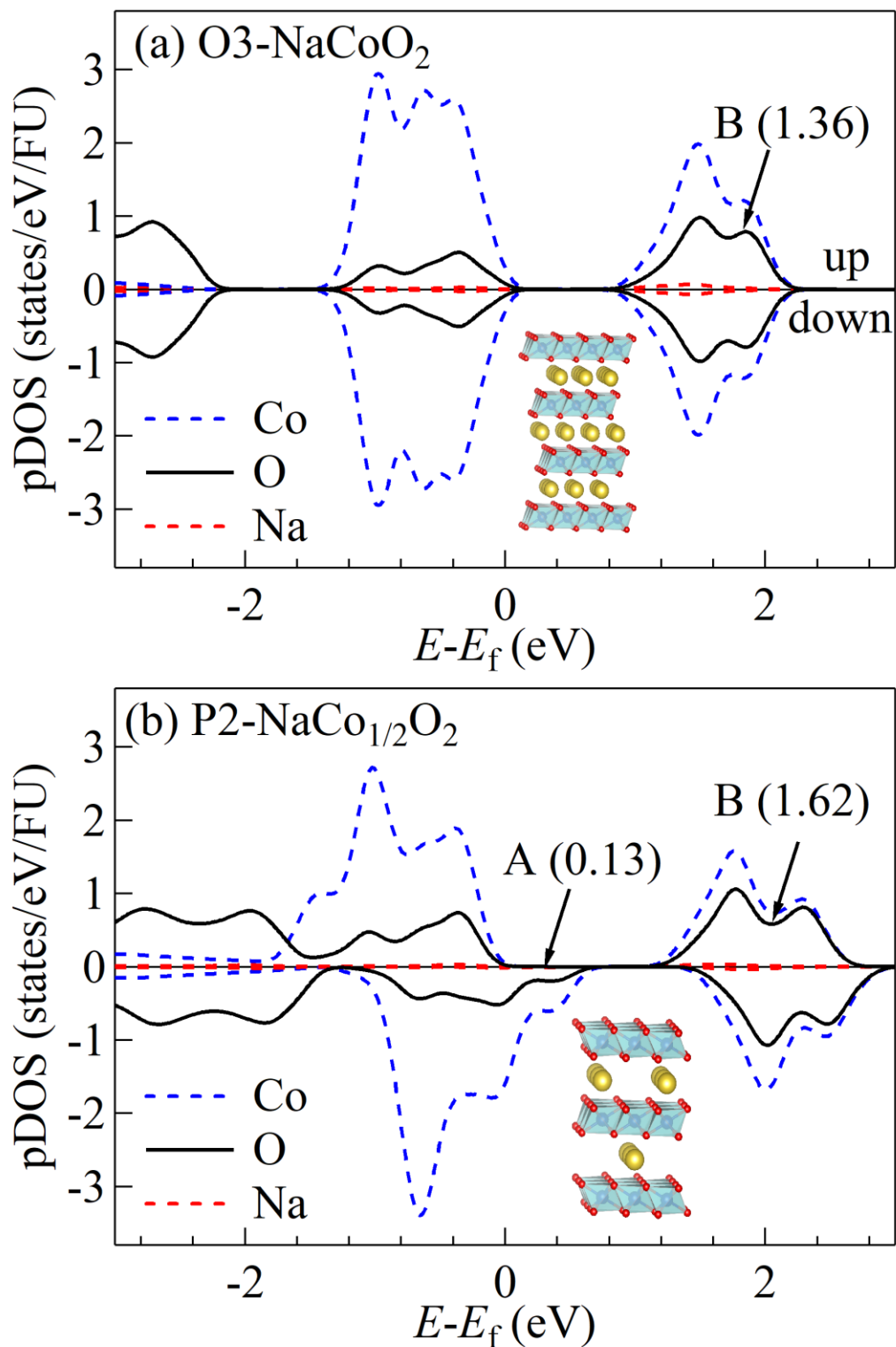


Figure 2. O K-edge spectra recorded in TEY mode of (a) O3- $\text{Na}_{0.91}\text{CoO}_2$  and (b) P2-

$\text{Na}_{0.66}\text{CoO}_2$  in the pre-edge region. The spectra were normalized to have the same total area (526 – 550 eV). Open circles are experimental data, dashed curves are backgrounds, black solid curves are fitted curves, red and blue solid curves are the least-squares fitting of each peak with Gauss functions. The numbers in the Figure represent the spectral weights of the peaks A', A and B, respectively. Inset shows schematic structures of O3- $\text{NaCoO}_2$  and P2- $\text{NaCoO}_2$ .



**Figure 3.** Calculated pDOS of (a) O3-NaCoO<sub>2</sub> and (b) P2-Na<sub>1/2</sub>CoO<sub>2</sub>. Numbers in the Figure represent the unoccupied pDOS intensities of the oxygen component. Inset shows

schematic structure of O3-NaCoO<sub>2</sub> and P2-Na<sub>1/2</sub>CoO<sub>2</sub>.